EUROPEAN JOURNAL OF BIOMEDICAL AND PHARMACEUTICAL SCIENCES
http://www.ejbps.com

ISSN 2349-8870
Volume: 7
Issue: 9
490-496
Year: 2020

SOL GEL DERIVED NANOSTRUCTURED MANGANESE OXIDE NANOCOMPOSITE FOR UREA SENSOR

N. H. Bansod*

Nanotechnology Research Laboratory, Shri Shivaji Science College, Amravati -444602, (MS) India.

***Corresponding Author: N. H. Bansod**
Nanotechnology Research Laboratory, Shri Shivaji Science College, Amravati -444602, (MS) India.

Article Received on 20/07/2020 **Article Revised on 10/08/2020** **Article Accepted on 01/09/2020**

ABSTRACT
In present study, Nanoparticles of Co doped MnO_2 of the composition $Co_xMn_{1-x}O_2$(x= 0.03, 0.05, 0.07, 0.09) have been successfully synthesized by sol–gel method. The structure and morphology of Co doped MnO_2 (CMO) nanocomposite has been characterized by X-ray diffraction, scanning electron microscopy and transmission electron microscopy. The particle size of Co doped MnO_2 was found to be 33 nm. The sol-gel derived biocompatible Co doped MnO_2 and chitosan was deposited on Au plate by spin Coating method. The urea biosensor was fabricated by immobilizing urease enzyme (Ur) on as synthesized CHIT/CMO/Au electrode. The bioelectrode showed good response time, low detection limit and low value of Michaelis–Menten constant (Km= 4.5mM) indicating that enhancement of activity of enzyme with nanocomposite.

KEYWORDS: Co doped MnO_2 (CMO) nanocomposite, Biosensor, Cyclic Voltammetry, EIS.

INTRODUCTION
The estimation of urea is of clinical interest since decreased urea concentration (normal range is 15-40 mg/dl) causes hepatic failure, nephritic syndrome and at the same time increased urea level in blood and urine causes renal failure, urinary tract obstruction, dehydration, shock, burns and gastrointestinal bleeding.[1-2] Therefore, urea determination is very important as to current scenario.

Further, manganese oxides (MnO_2) have concerned considerable research interest due to their characteristic physical and chemical properties and wide applications such as ion exchange, molecular adsorption, energy storage, catalysis, and biosensor.[3] Manganese oxides have established application in catalysis, ion exchange reactions, as cathode materials for rechargeable batteries[4] and as distinguish agents for magnetic resonance imaging (MRI). It has variable oxidation state (+1 to +7) as well as structural and chemical forms.

It was assumed that replacing a small fraction of cations in a host metal oxide with a different cation also known as doping can change the catalytic activity of the metal oxide catalyst. The doping can modify the chemical bonding at the surface of the host oxide, which may in turn modify its catalytic activity favorably. The active centers in such systems could be either the oxygen atoms near the dopant or the dopant itself. In the same context, the activity of MnO_2 could be further improved by dispersing transition elements such as Ag[5] and Cu[6-7] on its surface or mixing with cobalt to form spinel oxide.[8] As a result, bifunctional metal oxides are frequently superior to either single component metal oxide in the catalytic activity because of the intimate bonding and synergetic coupling effects between two components.[9-11] For instance, the Co-and Mn-based binary metal oxides have found electrochemical applications for their outstanding redox stability and excellent catalytic properties.[12–14]

On other hand biodegradable and biocompatible polymers are suitable for human use and can be prepared into particles of various sizes. Chitosan is a positively charged natural biodegradable and biocompatible polymer. It is a linear polysaccharide consisting of h-1, 4 linked monomers of glucosamine and N-acetyl glucosamine. There are numerous reports highlighting the low toxicity and biocompatibility of chitosan. In recent years, Chitosan was used commercially in the medical field, especially in biomedical and pharmaceutical applications.

Enzyme ureases functionally, belong to the super family of amidohydrolases and phosphotriesterases.[15] It is an enzyme that catalyzes the hydrolysis of urea into carbon dioxide and ammonia. The reaction occurs as follows:

$$(NH_2)_2CO + H_2O \rightarrow CO_2 + 2NH_3$$

More specifically, urease catalyzes the hydrolysis of urea to produce ammonia and carbamate; the carbamate

produced is subsequently degraded by spontaneous hydrolysis to produce another ammonia and carbonic acid.[16] Urease activity tends to increase the pH of its environment as it produces ammonia, a basic molecule.

Herein, we disclosed first synthesis of Co- doped MnO_2 nanocomposite by sol-gel citrate method. And its characterization by XRD, scanning electron microscopy (SEM) and transmission electron microscopy (TEM). Further immobilize the uresae enzyme on CHIT/CMO/Au plate by simple adsorption method. The proposed sensor demonstrated high sensitivity, wide linear range, high selectivity, good stability, and satisfactory feasibility for detection of urea in trace level.

2. EXPERIMENTAL

2.1 Chemicals and Reagents

Urease, Cobalt (II) nitrate hexahyadrate ($Co(NO_3)_2.6H_2O$), Manganese (II) nitrate hexahydrate, Urea, Citric acid, Ethanol, Potassium ferrocyanide, KCl were procured from S D Fine chemical limited, (SDFCL) (Mumbai, India.) All reagents were of analytical grade and used without further purification. All the solutions were prepared in deionized water.

2.2 Synthesis of Co doped MnO_2Nanocomposite

The Co doped MnO_2 ($Co_xMn_{1-x}O_2$)nanocomposite have been prepared by sol-gel citrate method.[17] Precursors (Manganese nitrate, Cobalt nitrate (3% 5% 7% and 9% by wt) and citric acid in stoichiometrically were grinded (mechanical process) using a mortar–pestle for 30 min for obtaining a homogenous mixture. The mixed powder was poured in beaker, add 50 ml of ethanol to it. Stir it constantly for 3 hrs at 80°C on magnetic stirrer to get homogeneous and transparent solution. This solution was further heated at about 130°C for 12 hrs in pressure bomb to form gel precursor. The resultant mixture is calcinated in muffle furnace at 350°C for 3 hrs. The dried powder was calcinated at 650°C for about 6 hrs. Crystallinity and sensitivity of the material can be achieved.

2.3 Preparation of CHIT/CMO/Au Electrode

Au plate was repeatedly rinsed with ethyl alcohol. Initially Chitosan a natural copolymer and sol-gel synthesized Co doped MnO_2 (CMO) (1:1 ratio) were dissolved in 100 ml 0.2M acetic acid by stirring at room temperature for 3 hrs. Finally a viscous solution of Chitosan-nano Co doped MnO_2 (CMO) was obtained. Pour the solution on previously washed Au plate uniformly by dip coating technique till the sufficient amount layer was deposited. A dried CHIT/CMO/Au electrode was washed repeatedly with 50 mM phosphate buffer solution.

2.4 Enzyme Immobilization on CHIT/CMO/Au Electrode

The immobilization of urease enzymes on CHIT-Co doped MnO_2 nanocopmposite deposited on Au plate was done using physical adsorption method. Ten micro liters (mL) of urease enzymes (1.0 mg/mL, in PB, 50 mM, pH 7.0) was immobilized onto a sol-gel CHIT/Co doped MnO_2(CMO)/Au electrode by the physisorption method.

As fabricated, the Urs-CHIT/Co doped MnO_2/Au bioelectrode was allowed to dry overnight under desiccated conditions and then washed with phosphate buffer solution (PBS, 50 mM, pH 7.0) to remove any unabsorbed enzymes and stored at 5°C when not in use.

2.5 Characterization

Phase identification of Co doped MnO_2 (CMO) Nanocomposite was accomplished by x-ray diffractometer using Cu K_α radiation (X-pert MPD, Philips, Holland) in the range 20-80 (2θ scale). The surface morphology of synthesized nanocomposite was examined by scanning electron microscopy (Nova-nano SEM-450) and transmission electron microscopy (Technai-20 Philips, Holland). The electrochemical data was obtained on CH instrument (CH instrument Electrochemical Analyzer Made in USA) by using three-electrode cell containing Ag/AgCl as reference electrode, platinum (Pt) wire as auxiliary electrode, and CHIT/Co doped MnO_2(CMO)/Au working electrode in PBS solution containing 5 mM $[Fe(CN)_6]^{3-/4-}$.

3. RESULTS AND DISCUSSION

3.1 XRD Pattern

Fig. 1 shows XRD diffraction patterns results obtained for the 9% by wt of Co doped MnO_2 and pure MnO_2nanocomposites synthesized by sol-gel process, annealed at 650°C. The phases showed major characteristics diffraction peaks with indices for calcinated Co doped MnO_2 (CMO) at 2θ values 28.8° (310), 36.4°(211), 49.8°(411) degree and 27.9°, 36.7°, 44.05°2θ values for undoped MnO_2 can be indexed to a pure tetragonal phase of α-MnO_2 (JCPDS 44-0141). The XRD pattern clearly indicates the good crystalline nature of the Co doped MnO_2 in comparison with the pure a MnO_2 sample.

The grain size of the 9 % wt of Co doped in MnO_2(CMO) was determined using Scherrer formula:

$$D=0.9\lambda/ \beta \cos\theta \quad \text{.....(1)}$$

Where, λ is the wavelength of x-rays used, β is the full width at half maximum and θ is the corresponding position. The estimated grain size from most intense peak at (211) with Bragg angle 36.48° was found to be 33 nm. The decreased in the particle size of 9% wt of Co doped in MnO_2 nanocomposite as compared to pure MnO_2 was attributed to smaller ionic radius of Co^{2+}(0.78 A°) ion replaced the Mn^{2+}(0.83 A°) ion in lattice.

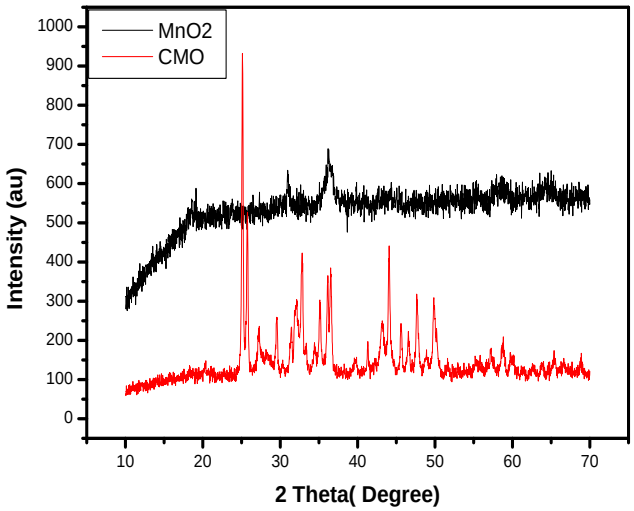

Fig. 1: XRD spectra of 9% wt of Co doped in MnO_2 (CMO) and pure MnO_2 calcinated at 650.°

3.2 Scanning Electron Microscopy

The morphology of Co doped MnO_2 was investigated by scanning electron microscopy. Fig.2 (A, B & C) shows a micrograph of Co doped MnO_2. It is clearly that the nanoclusters are composed of worm-like fibers aggregating on the surface of the nanosphere. These fibers appear more tightly packed and slightly smaller in size compared to the control sample. Their nanoporous structure, which offers very high specific surface area, promises good application in electrochemical properties. Again the surface morphology of nanoparticles reveals that uniform grain distribution suggesting the complete incorporation of Co in Co_x $Mn_{1-x}O_2$ lattice as supported by XRD. Furthermore no morphological alteration was observed in FESEM images.

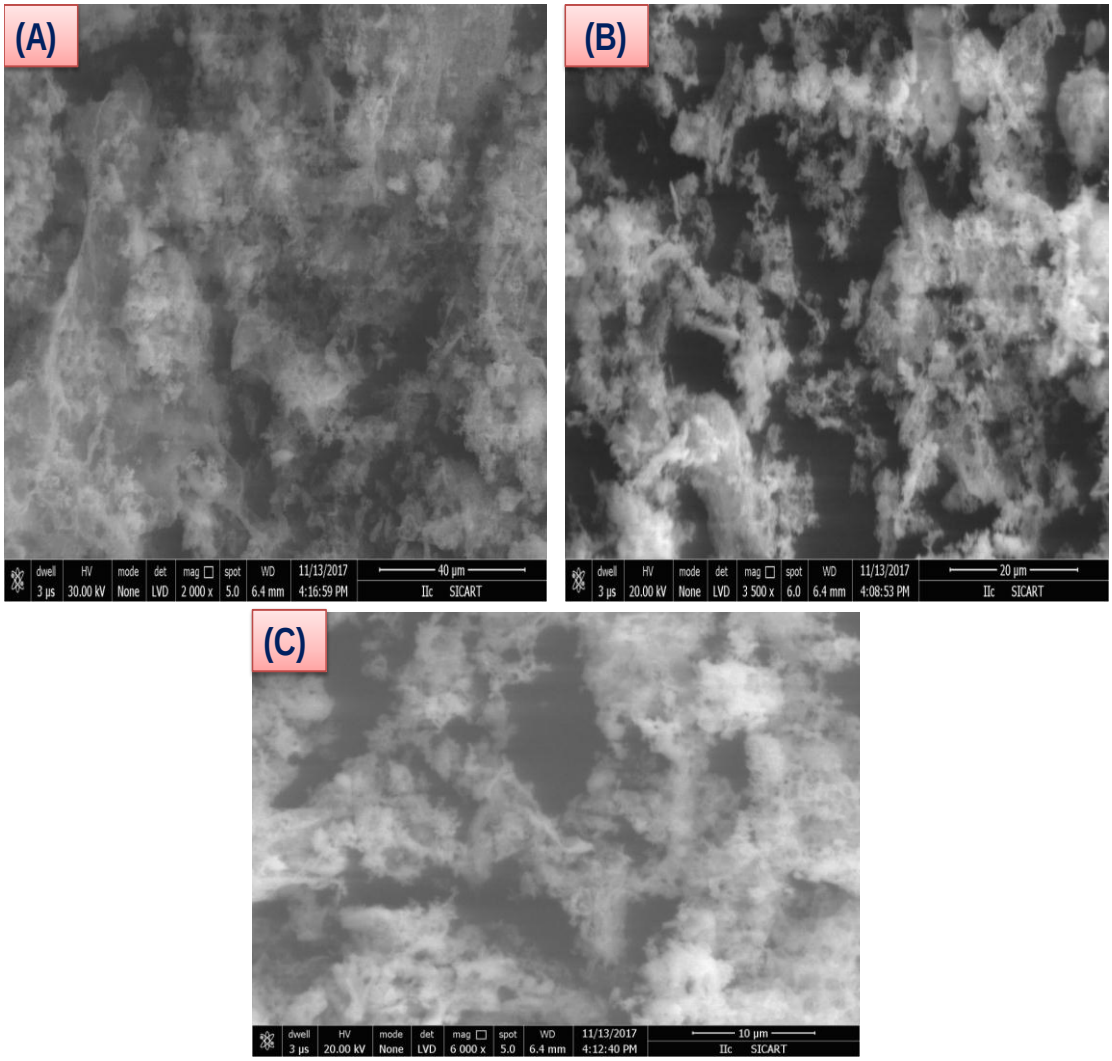

Figure 2: (A, B &C) at different magnification SEM micrograph of 9 % wt of Co doped MnO_2.

3.3 Transmission Electron Microscopy

The microstructure of the 9% wt of Co doped MnO_2 (CMO) was further examined with transmission electron microscopy as shown in the fig.3 (A&B) &(C&D) sample dispersed on TEM grids reveals hexagonal globular morphology with diameter 40-78.5 nm can be indexed as tetragonal α-MnO_2 type lattice.

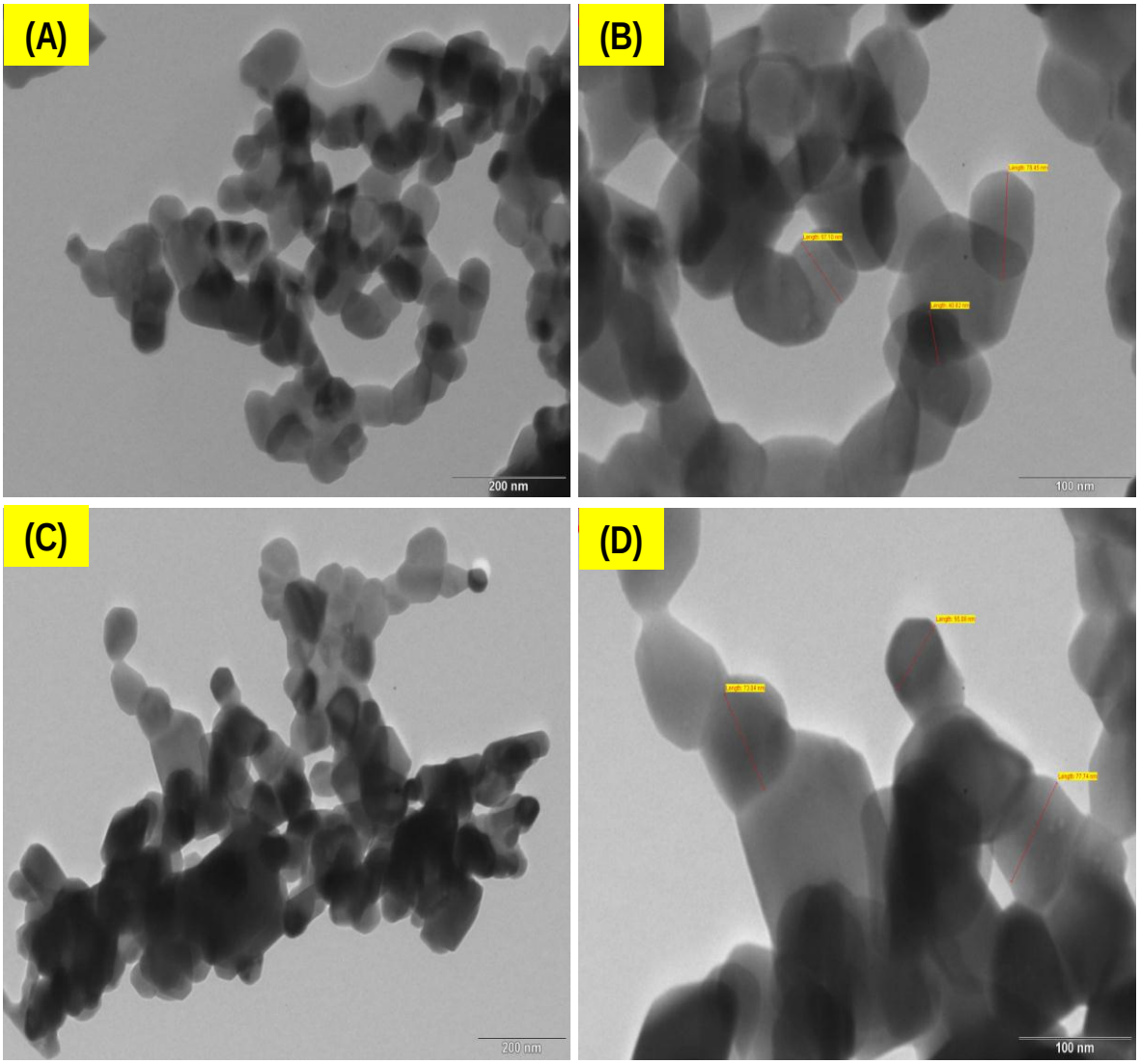

Fig.3 (A&B) Low resolution & (C&D) high resolution TEM micrograph of 9% wt of Co doped MnO_2.

3.4 Electrochemical Impedance Spectroscopy

Impedance spectroscopy is an effective means of probing the features of surface-modified electrodes. Nyquist plots are composed of a spike in the low frequency region and an incomplete semicircle in the high frequency region indicating a pronounced capacitive behavior with a moderate resistance.

The complex impedance can be presented as the sum of the real, Zre, and imaginary, Zim components that originate mainly from the resistance and capacitance of the cell, respectively. The general electronic equivalent circuit (Randles and Ershler model), includes the ohmic resistance of the electrolyte solution, Rs, the Warburg impedance, D, resulting from the diffusion of ions from the bulk electrolyte to the electrode interface. The double layer capacitance, Cdl, and charge-transfer resistance Rct exists, if a redox probe is present in the electrolyte solution.

Where Rs and D were denote bulk properties of the electrolyte solution and diffusion features of the redox probe in solution respectively. The other two components, Cdl and Rct, depend on the dielectric and insulating features at the electrode/electrolyte interface. Fig. 4.shows electrochemical impedance spectra EIS, Nyquist plot, curve (a) CHIT/MnO_2/Au electrode, Curve (b) CHIT/CMO/Au electrode and curve (c) Urs/CHIT/CMO/Au bioelectrode.

In the EIS, the semicircle diameter is equal to electron-transfer resistance Rct. The Rct value of CHIT/CMO/Au electrode decreases from 16.5 Ω to 15 Ω compared to CHIT/MnO_2/Au electrode, indicating that Co doped in MnO_2 nanocomposite result in enhanced electron transfer kinetics on nanocomposite electrode was attributed to Co^{2+} ion replaced Mn^{2+} ion in the lattice. Further Rct values, which were found to decrease with increase in Co content in the electrodes and confirming the influence of Co ion in the improvement of conductivity of the electrode as compared with CHIT/MnO_2.Moreover this result might be due to less favoring environment of CHIT/MnO_2 matrix for the effective entrapment of urease.[18]

After immobilization of Urs the Rct value increases to 17.5 Ω for Urs/CHIT/CMO/Au bioelectrode revealing

immobilization of Urs onto CHIT/MnO_2/Au matrix resulting in blocking of charge carriers in the nanobiocomposite.

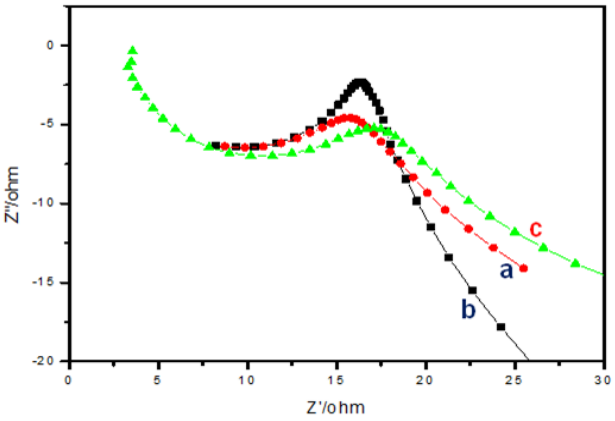

Fig. 4 : Nyquist plot, curve (a) CHIT/MnO_2/Au electrode, Curve (b)CHIT/CMO/Au electrode and curve (c) Urs/CHIT/CMO/Au bioelectrode.

3.5 Cyclic Voltammetry (CV)

Electrochemical study was performed in a three electrode cell configuration containing Urs/CHIT/CMO/Au (as the working electrode), Pt wire (as the counter) and Ag/AgCl (as the reference). Cyclic voltammetry (CV) was carried in the voltage in range -30 mV to 600 mV at the scan rate 10mVs^{-1}.The changes of electrode behavior after surface modification with enzymes (Urs) were studied by cyclic voltammetry (CV) in the presence of ferricyanide mediator.

Fig.5 shows the cyclic voltammograms for (a) bare Au electrode(b) CHIT/CMO/Au electrode (c)Urs/CHIT/ CMO/Au bioelectrode in PBS(50mM, pH 7.0,0.9% KCl) containing 5 mM $[Fe(CN)_6]^{3-/4-}$ at the scan rate of 10 mVs^{-1}.

The peak current of CHIT/CMO/Au electrode (4.6×10^{-4} A) (curve b) is less than that of bare Au electrode (6×10^{-4} A) (curve a) due to deposition of sol–gel derived insulating Co doped MnO_2 layer on the electrode surface that as a barrier to the interfacial electron transfer.

A well defined redox peak obtained for CHIT/CMO/Au electrode as compared to Urs/CHIT/CMO/Au bioelectrode. The peak current gradually decrease (0.00046 A to 0.0003A) (curve c) for bioelectrode due to physiorption of Urs on CHIT/CMO/Au electrode. At the same time peak to peak separation increase (ΔE_p) increases in the order bare Au electrode <CHIT/CMO/Au electrode < Urs/CHIT/CMO/ Au bioelectrode.The decreased in peak current could be attributed to electrostatic repulsion between oxidized Urease physisorbed on CHIT/CMO/Au electrode and anionic redox couple $[Fe(CN)_6]^{3-/4-}$ ions that are negatively charged.

In addition, redox potential, peak to peak separation (ΔE_p) increases for Urs/CHIT/CMO/Au bioelectrode is attributed to low electrical conductivity of enzyme and CHIT/CMO/Au electrode.

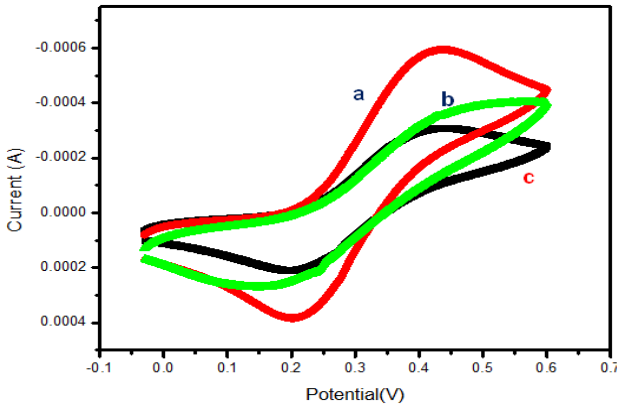

Fig.5: Cyclic voltammograms of a) bare Au electrode b) CHIT/CMO/Au electrode c) Urs/CHIT/CMO/Au bioelectrode at 0.01 scan rate.

3.6. Biosensor Response Study

Fig.6 (a) show the response studies of Urs/CHIT/CMO/Au bioelectrode with respect to addition of urea solution of different concentration (50-250 mg/ml) at an applied scan rate 10 mVs^{-1}. The peak current rises sharply with increased concentration of urea with the maximum response up to 250 mg/ml. This may be due to the increase in proton concentration in the electrolyte, which giving rise to larger current.[17] The biosensor achieves 90% of the steady current in less than 10 sec.

Fig. 6(b) shows the calibration plot from which detection of urea can be determined. It reveals that Urs/CHIT/CMO/Au bioelectrode had found two linear range, (10-150 mM) and (150-210 mM) with sensitivity of 0.01 µA mM^{-1}/cm^2 and 0.05 µA mM^{-1}/cm^2 respectively. The term Sensitivity, it can be defined as the ratio of the slope of the calibration curve to the active surface area of the working Au electrode. It is given by equation 2

$$\text{Sensitivity} = \frac{\text{Slope of the calibration curve}}{\text{Active suface area of the working electrode Au}} \quad \ldots\ldots(2)$$

The low detection limit (35mM) and linear regression coefficient of 0.988 and 0.909 were found out for bioelectrode.

Table 1 shows comparison of CMO modified electrode with other electrode.

Table 1: Comparison of analytical performance of the proposed electrode.

Enzymes	Immobilization matrix	Linear range	Limit of detection	Ref.
Urease	CeO2	10-100mg/ml	0.160 µM	20
Urease	CMO	10-150mM	35 mM	Present Work
Urease	Polyaniline –nafion Mno2	0.05-0.5 µM	0.05 µM	19

3.7 Determination of Km

The Michaelis–Menten constant (Km) was calculated by using linweaver–bruke equation 3

$$\frac{1}{Iss} = \frac{KmApp}{Imax}\frac{1}{C} + \frac{1}{Imax} \quad \ldots\ldots\ldots (3)$$

Where Iss is the steady-state current after the addition of substrate, C is the bulk concentration of the substrate, and Imax is the maximum current measured under saturated substrate condition. The slope of calibration cruve was found to be 0.05 and Imax value (maximum current) is $9x10^{-3}$ A. On the basis of this the Km value was found to be 4.5 mM. Which is a reflection of enzymatic affinity, the lower value of Km with respect to urease enzymes indicates that easier diffusion of substrate and product molecules into and out of CHIT/Co doped MnO_2 matrix.

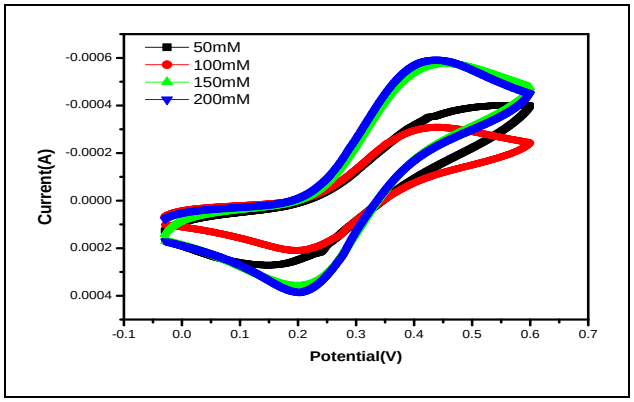

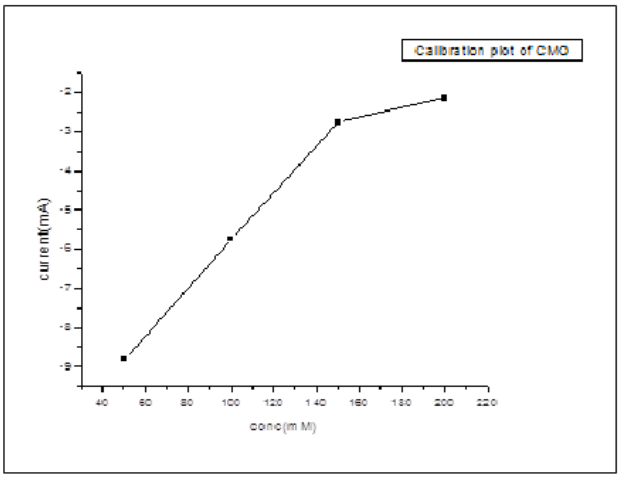

Fig. 6: (a) Electrochemical response of Urs/CHIT/CMO/Au bioelectrode with respect to concentration of urea (10-250 mM) at scan rate 10 mVs^{-1}. (b) Calibration plot of Urs/CHIT/CMO/ Au bioelectrode.

3.8 Effect of Potential Scan Rate

Fig.7. shows the influence of potential scan rate on oxidation reaction of urease at the CHIT/CMO/Au bioelectrode with scan rate varying from 10 to 100 mV/ s.

A linear relationship between the oxidation peak current and the scan rate showed predominantly adsorption control process. The proportional increase of redox current with respect to scan rate is observed due to diffusion-controlled system.

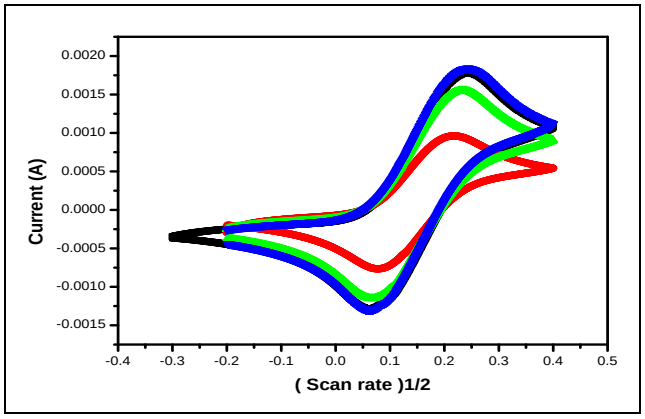

Fig. 7: CV of Urs/CHIT/CMO/Au bioelectrode at different scan rate.

3.8 Stability and Reproducibility

The storage stability of the Urs/CHIT/CMO/Au biosensor was about 6 days. After it the gradually decrease in response. Near about 20 days the biosensor shows significant response.

4. CONCLUSION

Co doped MnO_2 were prepared for different composition by sol-gel method. The considerable influence of Co doped on the spectroscopic characteristics and electrochemical properties are demonstrated. The XRD measurement exhibit a tetragonal structure for ($Co_xMn_{1-x}O_2$) at calcinations temperature 650°C. The crystalline size was decrease from ~43 to ~33 nm. The surface morphology of Co doped MnO_2 (CMO) nanocomposite was confirmed by TEM and SEM. Further the urea biosensor was fabricated by immobilizing urease enzyme onto CHIT/CMO/Au electrode by physical adsorption method. The biosensor exhibit excellent performance characteristics such as sensitivity (0.01 &0.05 µA $mM^{-1}cm^{-2}$), reproducibility wide linear range (10-250mM), and low detection limit (35mM). The Michaelis-Menten constant (Km) was found to be 4.5mM indicates high affinity of urease enzyme with the urea analyte.

REFERENCES

1. Ali A., Ansari A. A., Kaushik A., Solanki P. R., Barik A., Pandey M. K., and Malhotra B. D., Materials Letters, 2009; 63: 2473-2475.
2. Cho W.J. and Huang H., J. Anal. Chem, 1998; 703946-395.
3. Yan J.A., Khoo E.,Sumboja A.,Lee P. S., ACS Nano, 2010; 4: 4247-4255.
4. Deab M.S., Ohsaka T., Ange K., Chem. Int. Ed, 2006; 45: 5963-5966.
5. Xu R., Wang D., Zhou K., Li. Y., J. Catal, 2006; 237: 426.
6. Qian K., Qian Z., Hua Q., Jiang W., Appl. Surf. Sci, 2013; 273: 357.
7. Sadeghinia M., Rezaei E., Amini, Korean J. Chem. Eng, 2013; 30: 201.
8. Faure B., Alphonse P.,Appl. Catal. B: Environ, 2016; 180: 715.
9. Choi S.H., Kang Y.C., Chem. A Eur. J, 2014; 20: 3014–3018.
10. Indra A., Menezes P.W, Sahraie N.R., Bergmann A., Das C. M., Tallarida M., Schmeiber D.P., Strasser P., DriessM., J.Am. Chem. Soc, 2014; 136: 17530–17536.
11. Liang Y., Wang H. J., Zhou J. Y, Wang Li J., Wang T., Regier H., J. Am. Chem. Soc, 2012; 134: 3517–3523.
12. Ge X.,Liu Y., Goh F.T., Hor T.A., Zong Y., Xiao P., Zhang Z., Lim S.H., Wang Li. X., ACS Appl Mater Interfaces, 2014; 6: 12684–12691.
13. Kuo C. C., Lan W.J., Chen C.H., Nanoscale, 2014; 6: 334–341.
14. Kong D., Luo J., Wang Y. W., Ren W., Yu T., Luo Y., Yang Y., Cheng C.,Adv. Funct. Mater, 2014; 24: 3815–3826.
15. Holm L., Sander C., Proteins, 1997; 28: 72–82.
16. Zimmer M., J. Biomol Struct Dyn, 2000; 17: 787–97.
17. Chen L., Song Z., Liu G.,Liu W., Journal of Physics and Chemistry Solid, 2001; 74: 360-365.
18. Fabio A. D., Giorgi A. M., Soavi F., J Electrochem.Soc, 2001; 148: 845.
19. Do. J., Lin K., Ohara R., J Taiwan Inst. Chem Eng, 2011; 42: 662.
20. Anasari A.A., Sumana G., Pandey M.K., J Mater.Res, 2009; 24: 5.
21. Anasari A.A., Solanki P.R., Malhotra B.D., Applied Physics Letters, 2008; 92: 263901-903.